of δ_1^*,δ_2^*, and h; the vertical scale for γ was magnified four times in order to show the curvature better.

Close to $\varphi = 1$ the contribution to h, represented by the area under the curve of $(1 - \varphi)^2/\gamma$, is appreciably less than the contribution to either δ_1^* or δ_2^*. The gradient of the integrand in h is also much smaller in that region than the gradients of the integrands in δ_1^* and δ_2^*.

When Eqs. (11–13) are integrated numerically, an interval of $\Delta\varphi = 0.01$ generally gives high accuracy, although some solutions would need a slightly smaller value. The dependent variable γ behaves well and can be obtained accurately up to $\varphi = 0.99$, but soon after that high accuracy is difficult to achieve because $dg/d\varphi$ in Eq. (12) is then very large. No matter how accurate f_0'' may be, because of the singularity mentioned earlier, it is always difficult to make γ very small at $\varphi = 1$ where it should, in fact, be zero. Fortunately, however, the effect on h is negligible and the method gives $h(1) = (\delta_1^* - \delta_2^*)$ at least as accurately as the most accurate solutions found in the literature.

Most methods of integrating Eq. (4) give high accuracy when the velocity f' (or φ) is in the range $0 \leq f' \leq 0.99$, but

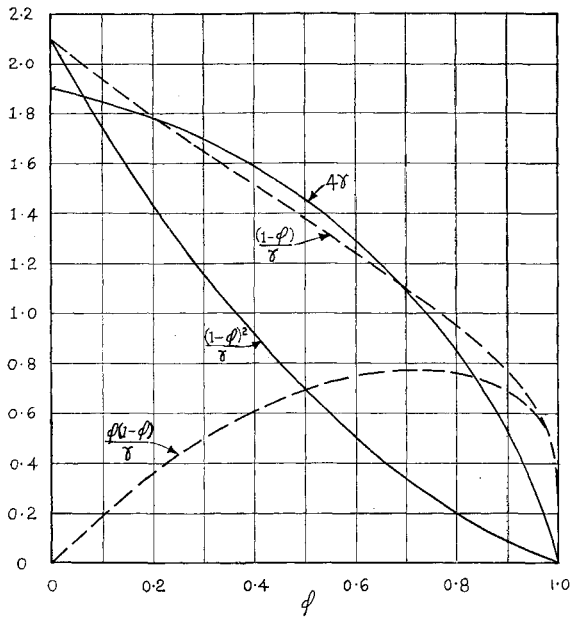

Fig. 1 Variation of 4 γ and the integrands in δ_1^*, δ_2^*, and h with the fluid velocity φ for the typical solution $\beta = 1.0$, $f_0 = -2.0$

some tend to break down between $f' = 0.99$ and $f' = 1.0$. The present method has the advantage that integration over this last interval can often be achieved in one step, and more than three steps would rarely be necessary.

The following method of completing the integration is also found to work well. The contribution to $(\delta_1^* - \delta_2^*)$ up to $\varphi = 0.98$ is given accurately by the integration process just described, as also are the values of γ at $\varphi = 0.98$ and $\varphi = 0.99$. Since the integrand in h is necessarily zero at $\varphi = 1.0$, the small contribution from the range $0.98 \leq \varphi \leq 1.0$ is evaluated readily by Simpson's rule.

As an example, the method was applied to the two-dimensional forward stagnation point with no fluid flowing through the wall. With the following data $\beta = 1.0$, $f_0 = 0$, $f_0'' = 1.2325877$, and $\Delta\varphi = 0.01$, the method gave $(\delta_1^* - \delta_2^*) = 0.3555568$. In order to obtain a solution of comparable accuracy by integrating Eq. (4) directly, the wall shear f_0'' was obtained to three more digits by trial and error. With $f_0'' = 1.232587604$ and an interval of $\Delta\eta = 10/128$ this method gave $(\delta_1^* - \delta_2^*) = 0.3555572$, where there is uncertainty about the last digit. The difference between the two values is clearly negligible.

References

[1] Spalding, D. B., "Mass transfer through laminar boundary layers, 1: The velocity boundary layer," Intern. J. Heat Mass Transfer **2**, 15–32 (1961).

[2] Watson, E. J., "Asymptotic theory of boundary layer flow with suction," Brit. Aeronaut. Res. Council, Res. and Memo. 2619 (1952).

[3] Eckert, E. R. G., Donoughe, P. L., and Moore, B. J., "Velocity and friction characteristics of laminar viscous boundary-layer and channel flow over surfaces with ejection or suction," NACA TN 4102 (1957).

[4] Spalding, D. B. and Evans, H. L., "Mass transfer through laminar boundary layers, 2: Auxiliary functions for the velocity boundary layer," Intern. J. Heat Mass Transfer **2**, 199–221 (1961).

Impulse Bit Measurement for Small Pulsed Rocket Motors

P. S. STARRETT* AND P. F. HALFPENNY†
Lockheed California Company, Burbank, Calif.

Conservation of propellants in attitude control for spacecraft often requires delivery of a low thrust in very short pulses. A method for measurement of the integrated impulse bit using a swinging pendulum is described. Some of the results in the successful application of this technique to an experimental program on cold gas propellants are presented.

DURING a research program on the performance attainable with selected cold gas propellants in an attitude control system, it was necessary to devise a method of determining the effective specific impulse for very short pulses. The work done covered pulse durations from 25 to 125 msec and thrusts of 1 to 10 lb, although the method is certainly adaptable to shorter pulses and smaller thrusts.

Load cell measurements of short pulses tend to become cluttered with extraneous oscillations of the system under test, making the data difficult to reduce. Also, inertial forces induced by closing and opening the valve solenoids produce confusing indications. Therefore, measurement of the integrated effect of the impulse bit appeared to be a desirable goal. Several methods of accomplishing this were examined. A technique finally was selected which involved measuring the impulse received by a swinging pendulum. The advantages of this approach were 1) all dynamic events occurring during the pulse were integrated and the net effect observed; 2) the measurement was essentially a primary one, depending only on a proper measurement and interpretation of the pendulum dynamics; and 3) the design and fabrication costs would be very modest.

Swinging Pendulum Technique

In the study of cold gas propellants, all components were supported on the pendulum, as shown in Fig. 1, and the pendulum was suspended by a crossed-pivot flexure from a rigid attachment. A knife edge support also was tried but resulted in higher decay rates. Instrumentation and control lines from the pressure and temperature transducers and the valve pulse circuit were brought through the plane of the flexure to minimize their effect on the pendulum performance.

The impulse imparted to the pendulum by a pulse could be evaluated either in terms of a change in pendulum ampli-

Received April 1, 1963.

* Group Engineer, Thermodynamic Systems Research. Member AIAA.

† Research Specialist, Thermodynamic Systems Research.

Table 1 Pendulum calibration

Gas stored[a]	Freon-14 at 1000 psi	Nitrogen at 1000 psi	Empty
Weight W, lb	39.2	37.1	36.5
Period t, sec	1.86	1.87	1.87
Center of gravity x, ft	1.928	1.992	2.010
Radius of gyration k_0, ft	2.33	2.389	2.398
Thrust line l_t, ft	3.98	3.98	3.98
Timing line l_p, ft	4.32	4.32	4.32

[a] Symbols refer to Fig. 1.

tude or by a change in the velocity at bottom dead center. The latter method was chosen as more adaptable to available equipment.

A pulse circuit was designed which applied a 24-v d.c. signal to the valve. The signal duration could be varied from 20 to 1400 msec. The pulse was triggered by interruption of a photo cell beam that occurred at bottom dead center of pendulum swing. The average velocity of the pendulum near bottom dead center was determined by interruption of the two timing photo cells. A digital electronic timer output was printed out for each swing of the pendulum. The actual change in velocity following a pulse was determined by plotting the time increments between the photo cells for a number of swings prior to and after the pulse and noting the displacement of these two curves. This method accounted for the natural velocity decay of the pendulum.

Pendulum Analysis

The equations of motion for the pendulum may be written by examining Fig. 1. Summing torques around the flexure,

$$\Sigma T = I_0\alpha = -W\bar{r}\sin\theta - Fl_t = (Wk_0^2/g)(d^2\theta/dt^2) \quad (1)$$

or

$$\ddot{\theta} + (\bar{r}g/k_0^2)\sin\theta + (Fl_tg/Wk_0^2) = 0 \quad (2)$$

where

I_0 = angular moment of inertia
α = angular acceleration
W = total pendulum weight
$\bar{r}$ = distance from fulcrum to center of gravity
l_t = distance from fulcrum to centerline of applied thrust
θ = angular displacement from bottom dead center
F = applied thrust
k_0 = pendulum radius of gyration
g = gravitational constant
t = time

Assuming for small angles $\sin\theta \approx \theta$ and grouping terms such that

$$A^2 = \bar{r}g/k_0^2 \qquad B = Fl_tg/Wk_0^2$$

Eq. (2) may be written as

$$\ddot{\theta} + A^2\theta + B = 0 \quad (3)$$

Laplace transform of this equation is

$$\theta(s) = \frac{s\theta_0}{s^2 + A^2} + \frac{\dot{\theta}_0}{s^2 + A^2} - \frac{B}{s(s^2 + A^2)} \quad (4)$$

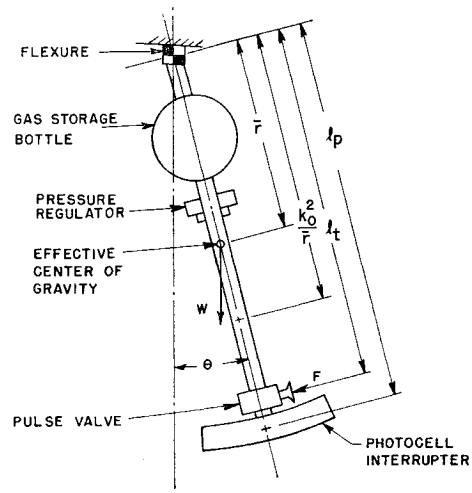

Fig. 1 Arrangement of pulsed pendulum

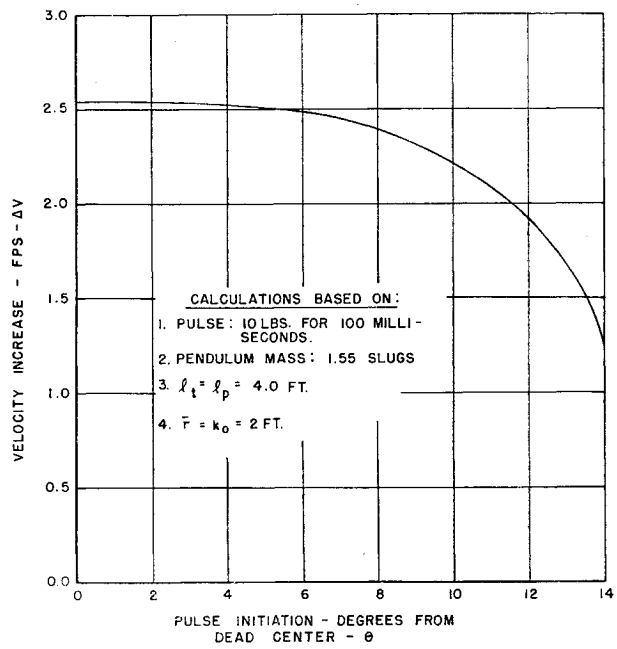

Fig. 2 Effect of pulse position on maximum velocity increase

where θ_0 and $\dot{\theta}_0$ are the angular displacement and velocity, respectively, at $t = 0$. The inverse transform of Eq. (4) is

$$\theta = \theta_0\cos At + (\dot{\theta}_0/A)\sin At - (B/A^2)(1 - \cos At) \quad (5)$$

and

$$\dot{\theta} = -\theta_0 A\sin At + \dot{\theta}_0\cos At - (B/A)\sin At \quad (6)$$

These equations assume a constant force over a short pulse. An analysis assuming a short pulse varying with time can be made by rewriting Eq. (3) to include $F(t)$ as a forcing function, and then introducing the unit impulse (delta) function.[1] However, such an analysis leads to the same working

Table 2 Typical performance data

	Pulse duration, msec					
	36.7		79.2		125.5	
	N_2	F-14	N_2	F-14	N_2	F-14
Velocity at bottom dead center before pulse, fps	2.74	2.82	2.18	2.736	1.012	1.855
Velocity at bottom dead center after pulse, fps	3.23	3.36	3.19	3.858	3.001	3.76
Impulse bit, lb-sec/pulse	0.1877	0.2065	0.387	0.430	0.761	0.730
Specific impulse, sec	68.6	43.0	69.5	43.5	68.5	43.0

equations for the pendulum if corresponding simplifying assumptions are made. In the pulsed pendulum tests, the increase in the maximum velocity at bottom dead center was used to deduce the thrust. The criticality of pulse position was examined analytically using Eqs. (5) and (6). This was done by permitting a free swing to a given position, starting a new solution at that point for pulsed operation with the free swing terminal boundary conditions $(\theta_0, \dot{\theta}_0)$, and then renewing the solution for free swing again with terminal boundary conditions from the pulsed period. The curve developed from this information (Fig. 2) indicated that for the conditions examined the measured velocity increase would be relatively insensitive to pulse position with $\pm 5°$ of bottom dead center. During the tests all pulses were initiated $\pm \frac{1}{4}°$ of bottom dead center. In reducing the data from this latter case, note that Eq. (6) with the initial condition $\theta_0 = 0$ becomes

$$\dot{\theta} = \dot{\theta}_0 \cos At - (B/A) \sin At \tag{7}$$

and, for small values of At, this becomes

$$\dot{\theta} - \dot{\theta}_0 = -Bt_p \tag{8}$$

where t_p = duration of pulse (valve open time). Thus, the measured velocity change (Δv) at bottom dead center before and after a pulse is

$$\Delta v = Bl_p\, t_p = (F_e t_p)\, l_l l_p\, g/Wk_0^2 \tag{9}$$

or

$$I_b = (F_e t_p) = Wk_0^2 \Delta v / l_l l_p g \tag{9a}$$

where I_b is the integrated impulse bit applied during a pulse and F_e is the "effective thrust" defined as

$$F_e \equiv I_b/t_p \tag{10}$$

Checks of the simplifying assumptions in Eq. (9a) indicate that errors greater than 1% are not introduced. In the tests v_{max} at bottom dead center was not measured but rather the average velocity over the distance between the photocells. This small correction can be defined precisely as a function of observed time increments. Appropriate corrections were applied to all data.

The radius of gyration was deduced from the natural period of the pendulum, and the center of gravity was determined experimentally. A slight shift in these quantities took place as gas was used from the bottle, but this was a small correction that was easy to apply. In Table 1, the characteristics of the pendulum actually used are given.

Pulsed Rocket Tests

Runs were made with the pendulum installed in an extreme altitude chamber. Swings were initiated by pulsing the valve, and data were recorded under a variety of pulse durations until the storage bottle charge was exhausted.

Specific impulse was determined by dividing the total impulse per pulse (I_b) by the flow of propellant per pulse. This latter value was obtained by an independent weighing calibration for a large number of pulses. Typical data from the program are given in Table 2.

Summary

The performance of small pulsed rocket motors can be measured effectively by using a swinging pendulum. The measurement fundamentally is grounded in well-defined pendulum behavior. Such a pendulum can be built inexpensively, with masses and lengths adjusted to produce the desired accuracy.

Reference

[1] Azeltine, J. A., *Transform Methods in Linear System Analysis* (McGraw-Hill Book Co. Inc., New York, 1958), p. 22.

Radial Viscous Free-Mixing

MARTIN H. STEIGER*
Polytechnic Institute of Brooklyn, Farmingdale, N. Y.

Introduction

VISCOUS laminar and turbulent compressible radial jets (i.e., motionless ambient) and wakes are investigated by a boundary-layer type of analysis with integral methods. A schematic diagram of radial free-mixing is presented in Fig. 1. The radial jet, for example, can be produced by two circular jets of equal strength, which are directed at one another and, after impact, spread out radially. Other types of radial free-mixing can be produced by flows issuing (or being absorbed) through perforations around the circumference of a right circular cylinder. Studies of radial flow have been restricted to laminar jets[1, 2] and laminar jets with an axisymmetric weak swirl.[2]

Analysis

The following boundary-layer equations are assumed to govern the viscous free-mixing previously discussed and represented schematically in Fig. 1:

Continuity

$$(\rho u x)_x + (\rho v x)_r = 0 \tag{1}$$

Momentum

$$\rho u u_x + \rho v u_r = (\mu u_r)_r \tag{2a}$$

$$p = \text{const} \tag{2b}$$

where x and r are the radial and normal coordinates with velocity components u and v, p denotes pressure, ρ density, μ coefficient of viscosity, and subscripts x and r denote partial differentiation with respect to the indicated variable.

Equations (1) and (2) govern either laminar flow or the mean quantities of turbulent flow if, in the turbulent case, the transport variable μ is interpreted to be the eddy coefficient of viscosity. Turbulent considerations are handicapped by a dearth of knowledge concerning the behavior of the eddy viscosity in compressible flows. Here it is suggested that the eddy viscosity may be assumed in the form

$$\epsilon_v = K \delta_m \rho_0 |u_e - u_0| \tag{3}$$

where K is a constant, δ_m is the transformed viscous layer thickness [Eq. (6)], and subscripts e and 0 denote conditions at the edge of the viscous-layer and quantities evaluated at the symmetric axis (i.e., at $r = 0$), respectively. In order to be able to treat both wakes and jets, the absolute value of $|u_e - u_0|$ should be taken. Equation (3) gives the proper behavior in the incompressible limit.

The boundary conditions are

$$\text{at } r = 0 \qquad u_r = v = 0 \tag{4a}$$

$$\text{at } r = \delta \qquad u = u_e = \text{const} \tag{4b}$$

Solutions are derived by applying the simple one-strip integral method, which consists of satisfying the momentum integral equation [derived by integrating (2) with respect to r and using Eqs. (1) and (4)], namely,

$$\int_0^\delta \rho u |u_e - u| x dr = \theta_c = \text{const} \tag{5a}$$

and the momentum equation evaluated along the x axis

$$\rho_0 u_0 (du_0/dx) = \mu_0 u_{rr_0} \tag{5b}$$

Received March 27, 1963. The study was supported partially by the Air Force Office of Scientific Research Grant No. AF-AFOSR-1-63.

* Research Associate, Graduate Center. Member AIAA.